

An Analytic Theory for the Orbits of Circumbinary Planets

Gene C. K. Leung¹ and Man Hoi Lee^{1,2}

ABSTRACT

Three transiting circumbinary planets (Kepler-16 b, Kepler-34 b, and Kepler-35 b) have recently been discovered from photometric data taken by the *Kepler* spacecraft. Their orbits are significantly non-Keplerian because of the large secondary-to-primary mass ratio and orbital eccentricity of the binaries, as well as the proximity of the planets to the binaries. We present an analytic theory, with the planet treated as a test particle, which shows that the planetary motion can be represented by the superposition of the circular motion of a guiding center, the forced oscillations due to the non-axisymmetric components of the binary's potential, the epicyclic motion, and the vertical motion. In this analytic theory, the periaapse and ascending node of the planet precess at nearly equal rates in opposite directions. The largest forced oscillation term corresponds to a forced eccentricity (which is an explicit function of the parameters of the binary and of the guiding center radius of the planet), and the amplitude of the epicyclic motion (which is a free parameter of the theory) is the free eccentricity. Comparisons with direct numerical orbit integrations show that this analytic theory gives an accurate description of the planetary motion for all three Kepler systems. We find that all three Kepler circumbinary planets have nonzero free eccentricities.

1. INTRODUCTION

Doyle et al. (2011) have recently discovered the first transiting circumbinary planet, Kepler-16 b, from photometric data taken by the *Kepler* spacecraft. The Saturn-mass planet orbits a pair of stars of $0.69M_{\odot}$ and $0.20M_{\odot}$. Welsh et al. (2012) subsequently announced the discovery of two more circumbinary planets: Kepler-34 b and Kepler-35 b. Kepler-34 b is $0.22M_J$ (where M_J is the mass of Jupiter) and orbits two Sun-like stars, while Kepler-35 b is $0.13M_J$ and orbits a pair of smaller stars ($0.89M_{\odot}$ and $0.81M_{\odot}$). For all three systems, the orbits of the binary and planet are aligned to within 2° . From the observed rate of circumbinary planets in their sample, Welsh et al. (2012) estimated that more than $\sim 1\%$ of close binary stars have giant planets on nearly coplanar orbits.

Variations in eclipse times and transit durations, combined with radial velocity measurements, allow precise measurements of both physical and orbital parameters for all three systems. Table 1

¹Department of Physics, The University of Hong Kong, Pokfulam Road, Hong Kong

²Department of Earth Sciences, The University of Hong Kong, Pokfulam Road, Hong Kong

shows the best-fit osculating Keplerian orbital parameters provided by J. A. Carter (2012, private communication). They differ slightly from those published in Table 1 of Welsh et al. (2012), as the values in that table are the medians of the cumulative distribution of the marginalized posteriors for each parameter, and they are osculating parameters at a different epoch.

Plots of the evolution of the osculating Keplerian orbital elements of the planets in the Supporting Online Material of Doyle et al. (2011) and Supplementary Information of Welsh et al. (2012) show significant variations on both orbital and secular timescales, with the eccentricity changing from nearly zero to 0.1 in the case of Kepler-16 b, and the precession period of the orbit is as short as ~ 60 orbital periods in the case of Kepler-35 b (see figures below for more details). The non-trivial departures from unperturbed Keplerian orbits for these circumbinary planets are due to the large secondary-to-primary stellar mass ratio ($m_B/m_A = 0.29\text{--}0.97$), the large orbital eccentricity of the binary $e_{AB} = 0.14\text{--}0.52$, and the proximity of the planet to the binary (orbital period ratio $P_b/P_{AB} = 5.6\text{--}10.4$).

In §2 we present an analytic theory for the orbit of a circumbinary planet that is valid in the limit that the planet has negligible mass and can be treated as a test particle. Lee & Peale (2006) have previously developed an analytic theory for the orbits of the small satellites of the Pluto-Charon system, assuming that the orbit of Charon relative to Pluto is circular. We generalize that theory to the case of an eccentric binary orbit. In §3 we present the results of direct numerical orbit integrations and compare them with the analytic theory. In §4 we discuss the limitations of the analytic theory and a simple modification that can significantly improve the analytic predictions when the orbital eccentricity of the binary is large. Our conclusions are summarized in §5.

2. ANALYTIC THEORY

In this section we follow a similar approach as Lee & Peale (2006) to develop an analytic theory for the orbit of a circumbinary planet. We extend their theory to first order in the eccentricity of the orbit of the binary. We assume that the planet has negligible mass and can be treated as a test particle. Then the orbit of the secondary (hereafter B) relative to the primary (hereafter A) is an elliptical Keplerian orbit with eccentricity e_{AB} and semimajor axis a_{AB} , and the distance between A and B is $r_{AB} = a_{AB}(1 - e_{AB}^2)/(1 + e_{AB} \cos f_B)$, where f_B is the true anomaly of B. We adopt a cylindrical coordinate system with the origin at the center of mass of the binary and the x - y plane being the orbital plane of the binary. The positions of B and A are $\mathbf{r}_B = (R_B, \phi_B, 0)$ and $\mathbf{r}_A = (R_A, \phi_B + \pi, 0)$, respectively, where $R_B = r_{AB}m_A/(m_A + m_B)$, $R_A = r_{AB}m_B/(m_A + m_B)$, m_A is the mass of A, and m_B is the mass of B.

2.1. Potential

The gravitational potential at $\mathbf{r} = (R, \phi, z)$ due to the binary is

$$\Phi(\mathbf{r}) = -\frac{Gm_A}{|\mathbf{r} - \mathbf{r}_A|} - \frac{Gm_B}{|\mathbf{r} - \mathbf{r}_B|}. \quad (1)$$

Since the orbit of the planet is nearly coplanar with that of the binary, we expand $1/|\mathbf{r} - \mathbf{r}_B|$ in powers of z :

$$\frac{1}{|\mathbf{r} - \mathbf{r}_B|} = \frac{1}{(\rho^2 + z^2)^{1/2}} = \frac{1}{\rho} - \frac{1}{2} \frac{z^2}{\rho^3} + \dots, \quad (2)$$

where

$$\rho = [R^2 + R_B^2 - 2RR_B \cos(\phi - \phi_B)]^{1/2}. \quad (3)$$

The inverse powers of ρ can be expressed as cosine series using equation (6.62) of Murray & Dermott (1999) to give

$$\frac{1}{|\mathbf{r} - \mathbf{r}_B|} = \frac{1}{2R} \sum_{k=0}^{\infty} (2 - \delta_{k0}) \left[b_{1/2}^k(R_B/R) - \frac{1}{2} \left(\frac{z}{R} \right)^2 b_{3/2}^k(R_B/R) + \dots \right] \cos k(\phi - \phi_B), \quad (4)$$

where δ_{k0} is the Kronecker delta and $b_s^k(R_B/R)$ are the Laplace coefficients. Similarly,

$$\frac{1}{|\mathbf{r} - \mathbf{r}_A|} = \frac{1}{2R} \sum_{k=0}^{\infty} (-1)^k (2 - \delta_{k0}) \left[b_{1/2}^k(R_A/R) - \frac{1}{2} \left(\frac{z}{R} \right)^2 b_{3/2}^k(R_A/R) + \dots \right] \cos k(\phi - \phi_B). \quad (5)$$

Then the potential can be written as

$$\Phi(\mathbf{r}) = \sum_{k=0}^{\infty} \left[\Phi_{0k}(R) - \frac{1}{2} \left(\frac{z}{R} \right)^2 \Phi_{2k}(R) + \dots \right] \cos k(\phi - \phi_B), \quad (6)$$

where

$$\begin{aligned} \Phi_{jk}(R) = & -\frac{2 - \delta_{k0}}{2} \left[(-1)^k \frac{m_A}{(m_A + m_B)} b_{(j+1)/2}^k(R_A/R) \right. \\ & \left. + \frac{m_B}{(m_A + m_B)} b_{(j+1)/2}^k(R_B/R) \right] \frac{G(m_A + m_B)}{R}. \end{aligned} \quad (7)$$

To first order in e_{AB} ,

$$\phi_B = f_B + \varpi_B \approx M_B + 2e_{AB} \sin M_B + \varpi_B, \quad (8)$$

where ϖ_B and $M_B = n_{AB}t + \varphi_{AB}$ are, respectively, the longitude of periapse and mean anomaly of B relative A, $n_{AB} = [G(m_A + m_B)/a_{AB}^3]^{1/2}$ is the mean motion of the binary, and φ_{AB} is a constant. Then

$$\begin{aligned} \cos k(\phi - \phi_B) \approx & \cos k(\phi - M_B - \varpi_B) + e_{AB}k[\cos(k(\phi - \varpi_B) - (k+1)M_B) \\ & - \cos(k(\phi - \varpi_B) - (k-1)M_B)]. \end{aligned} \quad (9)$$

To first order in e_{AB} ,

$$R_B/a_B \approx 1 - e_{AB} \cos M_B, \quad (10)$$

and

$$b_{(j+1)/2}^k(R_B/R) \approx b_{(j+1)/2}^k(\alpha_B) - e_{AB} \alpha_B D b_{(j+1)/2}^k(\alpha_B) \cos M_B, \quad (11)$$

where $a_B = a_{AB} m_A / (m_A + m_B)$, $\alpha_B = a_B / R$, and $D = d/d\alpha$. Equation (11) gives rise to terms involving

$$e_{AB} \cos M_B \cos k(\phi - \phi_B) = \frac{e_{AB}}{2} [\cos(k(\phi - \phi_B) + M_B) + \cos(k(\phi - \phi_B) - M_B)], \quad (12)$$

which can be expressed as

$$e_{AB} \cos(k(\phi - \phi_B) \pm M_B) \approx e_{AB} \cos(k(\phi - \varpi_B) - (k \mp 1)M_B). \quad (13)$$

Terms involving R_A/R can be found in a similar manner.

After re-grouping the terms,

$$\begin{aligned} \Phi(\mathbf{r}) = & \sum_{k=0}^{\infty} \left[\Phi_{0k0}(R) - \frac{1}{2} \left(\frac{z}{R} \right)^2 \Phi_{2k0}(R) + \dots \right] \cos k(\phi - M_B - \varpi_B) \\ & + e_{AB} \sum_{k=0}^{\infty} \left\{ k \left[\Phi_{0k0}(R) - \frac{1}{2} \left(\frac{z}{R} \right)^2 \Phi_{2k0}(R) + \dots \right] \right. \\ & \quad \left. - \frac{1}{2} \left[\Phi_{0k1}(R) - \frac{1}{2} \left(\frac{z}{R} \right)^2 \Phi_{2k1}(R) + \dots \right] \right\} \cos(k(\phi - \varpi_B) - (k+1)M_B) \\ & + e_{AB} \sum_{k=0}^{\infty} \left\{ -k \left[\Phi_{0k0}(R) - \frac{1}{2} \left(\frac{z}{R} \right)^2 \Phi_{2k0}(R) + \dots \right] \right. \\ & \quad \left. - \frac{1}{2} \left[\Phi_{0k1}(R) - \frac{1}{2} \left(\frac{z}{R} \right)^2 \Phi_{2k1}(R) + \dots \right] \right\} \cos(k(\phi - \varpi_B) - (k-1)M_B), \end{aligned} \quad (14)$$

where

$$\begin{aligned} \Phi_{jk0}(R) = & -\frac{2 - \delta_{k0}}{2} \left[(-1)^k \frac{m_A}{(m_A + m_B)} b_{(j+1)/2}^k(\alpha_A) \right. \\ & \left. + \frac{m_B}{(m_A + m_B)} b_{(j+1)/2}^k(\alpha_B) \right] \frac{G(m_A + m_B)}{R} \end{aligned} \quad (15)$$

and

$$\begin{aligned} \Phi_{jk1}(R) = & -\frac{2 - \delta_{k0}}{2} \left[(-1)^k \frac{m_A}{(m_A + m_B)} \alpha_A D b_{(j+1)/2}^k(\alpha_A) \right. \\ & \left. + \frac{m_B}{(m_A + m_B)} \alpha_B D b_{(j+1)/2}^k(\alpha_B) \right] \frac{G(m_A + m_B)}{R}. \end{aligned} \quad (16)$$

The terms in equation (14) multiplied by e_{AB} are new compared to the potential due to a binary on circular orbit derived by Lee & Peale (2006). As in the circular binary orbit case, the axisymmetric Φ_{j00} components of the potential are identical to those due to two rings: one of mass m_A and radius a_A and another of mass m_B and radius a_B .

2.2. Equations of Motion and Solution

The equations of motion in cylindrical coordinates are

$$\begin{aligned} \ddot{R} - R\dot{\phi}^2 &= -\frac{\partial\Phi}{\partial R}, \\ R\ddot{\phi} + 2\dot{R}\dot{\phi} &= -\frac{1}{R}\frac{\partial\Phi}{\partial\phi}, \\ \ddot{z} &= -\frac{\partial\Phi}{\partial z}. \end{aligned} \tag{17}$$

As in Lee & Peale (2006), we approximate the orbit of the circumbinary planet as small deviations from the circular motion of a guiding center in the x - y plane:

$$\begin{aligned} R &= R_0 + R_1(t), \\ \phi &= \phi_0(t) + \phi_1(t), \\ z &= z_1(t), \end{aligned} \tag{18}$$

where the constant R_0 is the radius of the guiding center, $|R_1/R_0| \ll 1$, $|\phi_1| \ll 1$, and $|z_1/R_0| \ll 1$.

Substituting equations (14) and (18) into equation (17), the only nontrivial equation at the zeroth order is

$$R_0\dot{\phi}_0^2 = \left[\frac{d\Phi_{000}}{dR} \right]_{R_0}, \tag{19}$$

which describes the circular motion of the guiding center. Its solution is

$$\phi_0(t) = n_0 t + \varphi_0, \tag{20}$$

where φ_0 is a constant and the mean motion n_0 is given by

$$\begin{aligned} n_0^2 &= \left[\frac{1}{R} \frac{d\Phi_{000}}{dR} \right]_{R_0} \\ &= \frac{1}{2} \left\{ \frac{m_A}{(m_A + m_B)} b_{1/2}^0(\alpha_A) + \frac{m_B}{(m_A + m_B)} b_{1/2}^0(\alpha_B) \right. \\ &\quad \left. + \frac{m_A m_B}{(m_A + m_B)^2} \left(\frac{a_{AB}}{R_0} \right) \left[D b_{1/2}^0(\alpha_A) + D b_{1/2}^0(\alpha_B) \right] \right\} n_K^2. \end{aligned} \tag{21}$$

In the above equation $n_K = [G(m_A + m_B)/R_0^3]^{1/2}$ is the Keplerian mean motion at R_0 , and α_A and α_B are evaluated at $R = R_0$.

At the first order, the equations of motion are

$$\begin{aligned}\ddot{R}_1 &= 2R_0 n_0 \dot{\phi}_1 - \left[\frac{d^2 \Phi_{000}}{dR^2} - n^2 \right]_{R_0} R_1 + e_{AB} \left[\frac{d\Phi_{001}}{dR} \right]_{R_0} \cos M_B \\ &\quad - \sum_{k=1}^{\infty} \left\{ \left[\frac{d\Phi_{0k0}}{dR} \right]_{R_0} \cos k(\phi_0 - M_B - \varpi_B) \right. \\ &\quad - e_{AB} \left[-k \frac{d\Phi_{0k0}}{dR} + \frac{1}{2} \frac{d\Phi_{0k1}}{dR} \right]_{R_0} \cos(k(\phi_0 - \varpi_B) - (k+1)M_B) \\ &\quad \left. - e_{AB} \left[k \frac{d\Phi_{0k0}}{dR} + \frac{1}{2} \frac{d\Phi_{0k1}}{dR} \right]_{R_0} \cos(k(\phi_0 - \varpi_B) - (k-1)M_B) \right\},\end{aligned}\quad (22)$$

$$\begin{aligned}\ddot{\phi}_1 &= -\frac{2n_0}{R_0} \dot{R}_1 + \sum_{k=1}^{\infty} \frac{k}{R_0^2} \left\{ \Phi_{0k0}(R_0) \sin k(\phi_0 - M_B - \varpi_B) \right. \\ &\quad - e_{AB} \left[-k\Phi_{0k0} + \frac{1}{2}\Phi_{0k1} \right]_{R_0} \sin(k(\phi_0 - \varpi_B) - (k+1)M_B) \\ &\quad \left. - e_{AB} \left[k\Phi_{0k0} + \frac{1}{2}\Phi_{0k1} \right]_{R_0} \sin(k(\phi_0 - \varpi_B) - (k-1)M_B) \right\},\end{aligned}\quad (23)$$

$$\ddot{z}_1 = \left[\frac{\Phi_{200}}{R^2} \right]_{R_0} z_1, \quad (24)$$

where $n = (R^{-1}d\Phi_{000}/dR)^{1/2}$ is the mean motion at R , and the quantities in the square brackets with the subscript R_0 are evaluated at $R = R_0$. Equation (23) can be integrated to give $\dot{\phi}_1$, which can then be substituted into equation (22) to yield

$$\begin{aligned}\ddot{R}_1 + \kappa_0^2 R_1 &= e_{AB} \left[\frac{d\Phi_{001}}{dR} \right]_{R_0} \cos M_B \\ &\quad - \sum_{k=1}^{\infty} \left\{ \left[\frac{d\Phi_{0k0}}{dR} + \frac{2n\Phi_{0k0}}{R(n - n_{AB})} \right]_{R_0} \cos k(\phi_0 - M_B - \varpi_B) \right. \\ &\quad - e_{AB} \left[-k \frac{d\Phi_{0k0}}{dR} + \frac{1}{2} \frac{d\Phi_{0k1}}{dR} + \frac{kn(-2k\Phi_{0k0} + \Phi_{0k1})}{R(kn - (k+1)n_{AB})} \right]_{R_0} \\ &\quad \times \cos(k(\phi_0 - \varpi_B) - (k+1)M_B) \\ &\quad - e_{AB} \left[k \frac{d\Phi_{0k0}}{dR} + \frac{1}{2} \frac{d\Phi_{0k1}}{dR} + \frac{kn(2k\Phi_{0k0} + \Phi_{0k1})}{R(kn - (k-1)n_{AB})} \right]_{R_0} \\ &\quad \left. \times \cos(k(\phi_0 - \varpi_B) - (k-1)M_B) \right\},\end{aligned}\quad (25)$$

where the epicyclic frequency κ_0 is given by

$$\kappa_0^2 = \left[R \frac{dn^2}{dR} + 4n^2 \right]_{R_0} \quad (26)$$

$$\begin{aligned}
= & \frac{1}{2} \left\{ \frac{m_A}{(m_A + m_B)} b_{1/2}^0(\alpha_A) + \frac{m_B}{(m_A + m_B)} b_{1/2}^0(\alpha_B) \right. \\
& - \frac{m_A m_B}{(m_A + m_B)^2} \left(\frac{a_{AB}}{R_0} \right) \left[D b_{1/2}^0(\alpha_A) + D b_{1/2}^0(\alpha_B) \right] \\
& - \frac{m_A m_B}{(m_A + m_B)^2} \left(\frac{a_{AB}}{R_0} \right)^2 \left[\frac{m_B}{(m_A + m_B)} D^2 b_{1/2}^0(\alpha_A) \right. \\
& \left. \left. + \frac{m_A}{(m_A + m_B)} D^2 b_{1/2}^0(\alpha_B) \right] \right\} n_K^2.
\end{aligned}$$

Equation (25) is the equation of motion of a simple harmonic oscillator of natural frequency κ_0 that is driven at frequencies n_{AB} , $k|n_0 - n_{AB}|$, and $|kn_0 - (k \pm 1)n_{AB}|$, and its solution gives

$$\begin{aligned}
R = & R_0 \left\{ 1 - e_{\text{free}} \cos(\kappa_0 t + \psi) - C_0 \cos M_B - \sum_{k=1}^{\infty} \left[C_k^0 \cos k(\phi_0 - M_B - \varpi_B) \right. \right. \\
& \left. \left. + C_k^+ \cos(k(\phi_0 - \varpi_B) - (k+1)M_B) + C_k^- \cos(k(\phi_0 - \varpi_B) - (k-1)M_B) \right] \right\}, \quad (27)
\end{aligned}$$

where e_{free} and ψ are arbitrary constants and

$$C_0 = -e_{AB} \left[\frac{d\Phi_{001}}{dR} \right]_{R_0} \bigg/ [R_0(\kappa_0^2 - n_{AB}^2)], \quad (28)$$

$$C_k^0 = \left[\frac{d\Phi_{0k0}}{dR} + \frac{2n\Phi_{0k0}}{R(n - n_{AB})} \right]_{R_0} \bigg/ \{ R_0 [\kappa_0^2 - k^2(n_0 - n_{AB})^2] \}, \quad (29)$$

$$\begin{aligned}
C_k^{\pm} = & e_{AB} \left[\pm k \frac{d\Phi_{0k0}}{dR} - \frac{1}{2} \frac{d\Phi_{0k1}}{dR} + \frac{kn(\pm 2k\Phi_{0k0} - \Phi_{0k1})}{R(kn - (k \pm 1)n_{AB})} \right]_{R_0} \bigg/ \\
& \{ R_0 [\kappa_0^2 - (kn_0 - (k \pm 1)n_{AB})^2] \}. \quad (30)
\end{aligned}$$

We can then solve equation (23) to give

$$\begin{aligned}
\phi = & n_0 t + \varphi_0 + \frac{2n_0}{\kappa_0} e_{\text{free}} \sin(\kappa_0 t + \psi) + \frac{n_0}{n_{AB}} D_0 \sin M_B \\
& + \sum_{k=1}^{\infty} \left[\frac{n_0}{k(n_0 - n_{AB})} D_k^0 \sin k(\phi_0 - M_B - \varpi_B) \right. \\
& + \frac{n_0}{kn_0 - (k+1)n_{AB}} D_k^+ \sin(k(\phi_0 - \varpi_B) - (k+1)M_B) \\
& \left. + \frac{n_0}{kn_0 - (k-1)n_{AB}} D_k^- \sin(k(\phi_0 - \varpi_B) - (k-1)M_B) \right], \quad (31)
\end{aligned}$$

where

$$D_0 = 2C_0, \quad (32)$$

$$D_k^0 = 2C_k^0 - \left[\frac{\Phi_{0k0}}{R^2 n(n - n_{AB})} \right]_{R_0}, \quad (33)$$

$$D_k^\pm = 2C_k^\pm - e_{AB} \left[\frac{k(\pm 2k\Phi_{0k0} - \Phi_{0k1})}{2R^2 n(kn - (k \pm 1)n_{AB})} \right]_{R_0}. \quad (34)$$

The motion in R and ϕ is the superposition of the circular motion of the guiding center at R_0 at frequency n_0 , the epicyclic motion represented by the *free* eccentricity e_{free} at frequency κ_0 , and the forced oscillations of fractional radial amplitudes C_0 , C_k^0 and C_k^\pm at frequencies n_{AB} , $k|n_0 - n_{AB}|$ and $|kn_0 - (k \pm 1)n_{AB}|$, respectively. Note that C_0 , C_k^0 , or C_k^\pm is singular if $\kappa_0^2 - n_{AB}^2$, $kn_0 - ln_{AB}$, or $\kappa_0^2 - (kn_0 - ln_{AB})^2 = 0$, where $l = k$ or $k \pm 1$. The second and third combinations of frequencies correspond to the corotation and Lindblad resonances, respectively (e.g., Goldreich & Tremaine 1980). None of these resonances could be encountered if the planet is further away than the 3:1 mean-motion resonance with the binary.

For the motion in z , the solution to equation (24) is

$$z = z_1 = R_0 i_{\text{free}} \cos(\nu_0 t + \zeta), \quad (35)$$

where i_{free} and ζ are arbitrary constants and the vertical frequency ν_0 is given by

$$\begin{aligned} \nu_0^2 &= \left[-\frac{\Phi_{200}}{R^2} \right]_{R_0} \\ &= \frac{1}{2} \left[\frac{m_A}{(m_A + m_B)} b_{3/2}^0(\alpha_A) + \frac{m_B}{(m_A + m_B)} b_{3/2}^0(\alpha_B) \right] n_K^2. \end{aligned} \quad (36)$$

Thus the motion in z decouples from that in R and ϕ and has only free oscillations represented by the *free* inclination i_{free} at the vertical frequency ν_0 .

As we shall see, circumbinary planets have $\nu_0 > n_0 > n_K > \kappa_0$. So the azimuthal period $2\pi/n_0$ is shorter than the Keplerian orbital period $2\pi/n_K$, the periape precesses in the prograde direction with the period $2\pi/|n_0 - \kappa_0|$, and the ascending node precesses in the retrograde direction with the period $2\pi/|n_0 - \nu_0|$.

As in the circular binary orbit theory of Lee & Peale (2006), the motion is represented by the circular motion of the guiding center, the epicyclic motion, the forced oscillations and the vertical motion. The expressions for the mean motion n_0 (eq. [21]), the epicyclic frequency κ_0 (eq. [26]), and the vertical frequency ν_0 (eq. [36]) involve the axisymmetric Φ_{000} and Φ_{200} components of the potential and are identical to those in the circular binary orbit case (there are, however, corrections at the second order in e_{AB} ; see §4). The motion in z is identical to the circular binary orbit case. The forced oscillations are composed of both terms identical to those in the circular binary orbit theory (C_k^0 at frequencies $k|n_0 - n_{AB}|$) and new terms (C_0 at frequency n_{AB} and C_k^\pm at frequencies $|kn_0 - (k \pm 1)n_{AB}|$). Note that the new terms C_0 and C_k^\pm are proportional to e_{AB} and that one of these terms, C_1^- , has frequency n_0 and can be identified as the *forced* eccentricity. The *forced* longitude of periape is aligned with the binary's periape because $C_1^- \geq 0$.

If we expand the analytic expressions in powers of a_{AB}/R_0 (note that $a_{AB}/R_0 \lesssim 0.32$ for the three Kepler systems) and retain only the lowest order term, we find that the precession rates

$$\frac{n_0 - \kappa_0}{n_K} \approx -\frac{n_0 - \nu_0}{n_K} \approx \frac{3}{4} \frac{m_A m_B}{(m_A + m_B)^2} \left(\frac{a_{AB}}{R_0} \right)^2, \quad (37)$$

the forced eccentricity

$$C_1^- \approx \frac{5}{4} e_{AB} \frac{(m_A - m_B)}{(m_A + m_B)} \left(\frac{a_{AB}}{R_0} \right), \quad (38)$$

and the other forced oscillation terms (up to $k = 3$)

$$C_2^0 \propto \frac{m_A m_B}{(m_A + m_B)^2} \left(\frac{a_{AB}}{R_0} \right)^5, \quad (39)$$

$$C_0, C_2^\pm \propto e_{AB} \frac{m_A m_B}{(m_A + m_B)^2} \left(\frac{a_{AB}}{R_0} \right)^5, \quad (40)$$

$$C_1^0, C_3^0 \propto \frac{m_A m_B (m_A - m_B)}{(m_A + m_B)^3} \left(\frac{a_{AB}}{R_0} \right)^6, \quad (41)$$

$$C_1^\pm, C_3^\pm \propto e_{AB} \frac{m_A m_B (m_A - m_B)}{(m_A + m_B)^3} \left(\frac{a_{AB}}{R_0} \right)^6. \quad (42)$$

We can see from equations (29) and (30) that C_k^0 and C_k^\pm involve Φ_{0k0} , Φ_{0k1} , and their derivatives with respect to R . According to equations (15) and (16), these terms would be exactly zero if k is odd and $m_A = m_B$. Equations (38), (41), and (42) show that the odd terms are proportional to $(m_A - m_B)/(m_A + m_B)$ at the lowest order in a_{AB}/R_0 and could be small if $m_A \approx m_B$.

3. COMPARISONS WITH NUMERICAL ORBIT INTEGRATIONS

For the numerical orbit integrations, we use Jacobi coordinates (where the position of the secondary B is relative to the primary A and the position of the planet is relative to the center of mass of the binary), with the invariable plane as the reference plane. This coordinate system reduces to that used in §2 when the mass of the planet is negligible. We perform direct numerical orbit integrations of the Kepler-16, 34, and 35 systems, using the Wisdom & Holman (1991) symplectic integrator with the modification described in Lee & Peale (2003). The modification allows the integration of circumbinary planets without an excessively small timestep, and we use a timestep of 0.1 day. We generate the initial positions and velocities of the binary and planet by using the best-fit osculating orbital parameters in Table 1.

For comparison with the analytic theory, we need to evaluate n_K , n_0 , κ_0 , ν_0 , and the fractional amplitudes C_0 , C_k^0 , and C_k^\pm at a guiding center radius R_0 . For each system, we adopt the average of the maximum and minimum values of the cylindrical radius R of the planet's orbit in the numerical orbit integration over many precession cycles as R_0 . The adopted R_0 and the numerical values of n_K , n_0/n_K , κ_0/n_K , ν_0/n_K , C_0 , C_k^0 , and C_k^\pm ($k = 1, 2$, and 3) are listed in Table 2.

3.1. Kepler-16

In Figure 1 we plot the evolution of the osculating Keplerian orbital elements of the planet Kepler-16 b over 100 years from the numerical orbit integration. The eccentricity e_b shows variations on both orbital and apsidal precession timescales. The longitude of periapse ϖ_b changes rapidly when e_b is nearly zero, but the long-term trend is prograde precession with a period of 48.6 years. The precession of the longitude of ascending node Ω_b is retrograde with a period of 41.0 years, and the inclination i_b shows small oscillations around a constant value, with two oscillations per nodal precession period. Using n_K , n_0/n_K , κ_0/n_K , and ν_0/n_K from Table 2, the analytic theory predicts that the apsidal and nodal precessions are at nearly equal rates in opposite directions, with the prograde apsidal precession having a period of 42.2 years and the retrograde nodal precession having a period of 42.8 years. These are in good agreement with the numerical results but slightly shorter for the apsidal precession and longer for the nodal precession.

In the bottom panels of Figure 2 we plot the variations in the orbital radius R_b of the planet Kepler-16 b over 5.4 years and 100 years. Significant periodic variations in the amplitude of the oscillations in R_b are observed from the 100-year plot. The variations have a period of 48.6 years, which is equal to the period of apsidal precession. The variations are the result of the superposition of the epicyclic motion at frequency κ_0 with amplitude e_{free} and the forced oscillation at frequency n_0 with amplitude C_1^- . Without any loss of generality, we can assume that both e_{free} and $C_1^- \geq 0$. After some algebraic manipulation using sum and product formulae of trigonometric functions, these two terms in equation (27) can be written as

$$\begin{aligned} & e_{\text{free}} \cos(\kappa_0 t + \psi) + C_1^- \cos(\phi_0 - \varpi_B) \\ &= e_{\text{free}} \cos(\kappa_0 t + \psi) + C_1^- \cos(n_0 t + \varphi_0 - \varpi_B) \\ &= (C_1^- + e_{\text{free}}) \cos\left(\frac{\varpi_{\text{free}} - \varpi_B}{2}\right) \cos\left[\frac{(n_0 + \kappa_0)t + \varphi_0 - \varpi_B + \psi}{2}\right] \\ &\quad - (C_1^- - e_{\text{free}}) \sin\left(\frac{\varpi_{\text{free}} - \varpi_B}{2}\right) \sin\left[\frac{(n_0 + \kappa_0)t + \varphi_0 - \varpi_B + \psi}{2}\right], \end{aligned} \quad (43)$$

where $\varpi_{\text{free}} = (n_0 - \kappa_0)t + \varphi_0 - \psi$ is the *free* longitude of periapse. A maximum amplitude is reached when $\varpi_{\text{free}} - \varpi_B = 2\ell\pi$ (where ℓ is an integer), in which case the right-hand side of equation (43) becomes $\pm(C_1^- + e_{\text{free}}) \cos\{[(n_0 + \kappa_0)t + \varphi_0 - \varpi_B + \psi]/2\}$. Similarly, a minimum amplitude is reached when $\varpi_{\text{free}} - \varpi_B = (2\ell + 1)\pi$, in which case the right-hand side of equation (43) becomes $\pm(C_1^- - e_{\text{free}}) \sin\{[(n_0 + \kappa_0)t + \varphi_0 - \varpi_B + \psi]/2\}$. Therefore, a maximum (or minimum) amplitude is reached every $2\pi/|n_0 - \kappa_0|$, which is equal to the apsidal precession period. The small minimum amplitude and large variations in the amplitude observed in the 100-year plot indicate that $e_{\text{free}} \sim C_1^-$.

The 5.4-year plot in the lower left panel of Figure 2 clearly shows an increase in the amplitude of the oscillations in R_b at the initial epoch due to the changing relative phase between the free and forced eccentricity terms, as well as higher-frequency forced oscillations. In order to study in more detail the forced oscillations and epicyclic motion, we plot in the upper panels of Figure 2 a

transformed orbital radius defined by

$$R' = R + R_0 \left\{ C_0 \cos M_B + \sum \left[C_k^0 \cos k(\phi_0 - M_B - \varpi_B) + C_k^+ \cos(k(\phi_0 - \varpi_B) - (k+1)M_B) + C_k^- \cos(k(\phi_0 - \varpi_B) - (k-1)M_B) \right] \right\}, \quad (44)$$

with R_0 , C_0 , C_k^0 , and C_k^\pm from Table 2 and ϕ_0 , M_B , and ϖ_B from the numerical integration itself (which eliminates phase errors due to small frequency errors and the very slow precession of the binary’s periape). It is clear from a comparison between the upper and lower panels of Figure 2 that the forced oscillations (including the forced eccentricity term) are sufficiently close to those predicted by the analytic theory that they are effectively eliminated in R'_b . The largest forced oscillation term, other than the forced eccentricity term, is C_2^- with a fractional amplitude of 0.0024 and a period of $2\pi/(2n_0 - n_{AB}) = 64.5$ days, and the other forced oscillation terms are at least a factor of 4 smaller in amplitudes. The free eccentricity can be easily obtained from R'_b , which shows only periodic epicyclic variation at frequency κ_0 . The forced and free eccentricities of Kepler-16 b are $C_1^- = 0.036$ and $e_{\text{free}} = 0.030$, respectively.

Having obtained e_{free} , which is a free parameter of the analytic theory, we can now directly plot the evolution of R according to equation (27) of the analytic theory (Fig. 3), as well as the evolution of the osculating Keplerian elements using R from equation (27), ϕ from equation (31), and their time derivatives (Fig. 4). They are in excellent agreement with the numerical orbit integration shown in Figures 1 and 2, except for the faster periape precession (and hence faster periodic variations in the radial oscillation amplitude), the slower nodal precession, and the lack of periodic variations in the inclination. Our analytic theory only gives the free oscillations in the vertical direction and cannot explain the periodic variations in the inclination at twice the nodal precession rate. For the eccentricity variations, if we ignore the higher-frequency forced oscillations, equation (43) shows that the osculating eccentricity reaches a maximum of $C_1^- + e_{\text{free}} = 0.066$ when the free longitude of periape ϖ_{free} is aligned with the forced longitude of periape (which is equal to the longitude of periape of the binary ϖ_B ; see §2.2), and reaches a minimum of $|C_1^- - e_{\text{free}}| = 0.006$ when the free longitude of periape ϖ_{free} is anti-aligned with the forced longitude of periape. This behavior agrees with the usual definitions of the forced and free eccentricities and longitudes of periape (see, e.g., Section 7.4 of Murray & Dermott 1999).

3.2. Kepler-34

Figures 5 and 6 show the evolution of the osculating Keplerian orbital elements, the orbital radius R_b and the transformed orbital radius R'_b of the planet Kepler-34 b. The periods of prograde apsidal precession and retrograde nodal precession are 62.9 and 67.9 years, respectively, from the numerical orbit integration. The analytic theory predicts 91.1 and 91.9 years, respectively, which are longer than the numerical results by more than 35%. The main reason for the large discrepancy

is that the analytic theory is only accurate to first order in the binary eccentricity e_{AB} and Kepler-34 has the largest $e_{AB}(= 0.52)$ among the three systems. We shall derive in §4 simple corrections at the second order in e_{AB} that significantly improve the analytic predictions of the precession periods.

One might think that the large osculating Keplerian eccentricity ($e_b \sim 0.2$) is due to forcing by the eccentric binary. But the nearly identical plots of R_b and R'_b show that the variations in R_b are primarily due to epicyclic motion and that the forced eccentricity C_1^- and other forced oscillation terms are small. Indeed, $C_1^- = 0.0019$, which is smaller than that for Kepler-16 b by more than an order of magnitude, and the next largest forced oscillation term is $C_2^- = 0.00068$ (see Table 2). The forced eccentricity C_1^- , as well as all C_k^0 and C_k^\pm terms with odd k , are small because of the nearly equal masses of the binary components of Kepler-34 ($m_B/m_A = 0.97$; see discussion in the last paragraph of §2.2). We find from the variations in R'_b that the free eccentricity $e_{\text{free}} = 0.204$.

3.3. Kepler-35

For Kepler-35 which has binary eccentricity ($e_{AB} = 0.14$) similar to Kepler-16, the numerical and analytic apsidal and nodal precession periods of the planet are in good agreement. The numerically determined apsidal and nodal precession periods are 21.7 and 20.2 years, respectively (see Fig. 7), and the analytic ones are 20.4 and 20.8 years, respectively.

As in the case of Kepler-34, the binary components have nearly equal masses ($m_B/m_A = 0.91$) and the forced eccentricity of the planet $C_1^- = 0.0025$ is small. However, because the free eccentricity is much smaller than that for Kepler-34 b and comparable to that for Kepler-16 b, moderate variations in the amplitude of oscillations in R_b with the same period as the apsidal precession are clearly observed in the 100-year plot in the lower right panel of Figure 8. The 4-year plot in the lower left panel of Figure 8 also shows the effects of higher-frequency forced oscillations terms. As for Kepler-16 b and 34 b, C_2^- is the largest forced oscillation term after the forced eccentricity term C_1^- (see Table 2). The forced oscillations are sufficiently close to those predicted by the analytic theory that the transformed orbital radius R'_b shows only periodic epicyclic variation at frequency κ_0 (see upper panels of Fig. 8). The free eccentricity from the variations in R'_b is $e_{\text{free}} = 0.038$.

4. DISCUSSION

The analytic theory developed in §2 is accurate to first order in the binary eccentricity e_{AB} and to first order in the deviations R_1 , ϕ_1 , and z_1 of the planetary motion from the circular motion of the guiding center. It also treats the planet as a test particle and ignores the gravitational effects of the planet on the motion of the binary. From the comparisons with direct numerical orbit integrations of the Kepler-16, 34, and 35 systems in §3, we have shown that the analytic theory

gives an accurate description of the planetary motion in all three cases, except for the apsidal and nodal precession periods of Kepler-34 b with $e_{AB} = 0.52$.

It was pointed out in §2 that the expressions for the mean motion n_0 (eq. [21]), the epicyclic frequency κ_0 (eq. [26]), and the vertical frequency ν_0 (eq. [36]) involve the axisymmetric Φ_{000} and Φ_{200} components of the potential and that the axisymmetric components of the potential are identical to those due to two rings: one of mass m_A and radius a_A and another of mass m_B and radius a_B . If we expand R_B/a_B to higher orders in e_{AB} (see eq. [2.81] of Murray & Dermott 1999),

$$\frac{R_B}{a_B} = 1 - e_{AB} \cos M_B + \frac{e_{AB}^2}{2}(1 - \cos 2M_B) + \frac{3e_{AB}^3}{8}(\cos M_B - \cos 3M_B) + \dots, \quad (45)$$

which means that the time-averaged $R_B/a_B = 1 + e_{AB}^2/2$ and that it might be more appropriate for the axisymmetric components of the potential to be due to two rings of radii $a_A(1 + e_{AB}^2/2)$ and $a_B(1 + e_{AB}^2/2)$. This is achieved if we selectively include just the $e_{AB}^2/2$ term beyond first order in e_{AB} and use $R_B/a_B \approx 1 - e_{AB} \cos M_B + e_{AB}^2/2$ (and similarly for R_A/a_A). Then the only modifications to the analytic theory in §2 are that $b_{(j+1)/2}^k(\alpha_A)$ is replaced by $b_{(j+1)/2}^k[\alpha_A(1 + e_{AB}^2/2)]$, and $b_{(j+1)/2}^k(\alpha_B)$ by $b_{(j+1)/2}^k[\alpha_B(1 + e_{AB}^2/2)]$, in equation (15) for Φ_{jk0} , and similarly for $Db_{(j+1)/2}^k(\alpha_A)$ and $Db_{(j+1)/2}^k(\alpha_B)$ in equation (16) for Φ_{jk1} . With this simple modification, the analytic predictions for the apsidal and nodal precession rates are faster than the unmodified values by only 2–3% for Kepler-16 b and 35 b, but by $\sim 29\%$ for Kepler-34 b. The increase by approximately $(1 + e_{AB}^2/2)^2$ can be understood from the $(a_{AB}/R_0)^2$ scaling of the lowest order expression for the precession rates in equation (37). The modified analytic precession periods for Kepler-34 b are 71.4 years for periapse and 72.1 years for ascending node, which are much closer to the numerical results (62.9 and 67.9 years, respectively) than the unmodified values (~ 91 years).

The $1 + e_{AB}^2/2$ modification also affects the amplitudes of the forced oscillation terms. The change in the largest of these, the forced eccentricity C_1^- , is small: $\lesssim 6\%$ even for Kepler-34 b. The change in the second largest forced oscillation term, C_2^- , is approximately $1 + 5e_{AB}^2/6$, which is only 2% for Kepler-16 b and 35 b but $\sim 24\%$ for Kepler-34 b. However, as we saw in §3.2, both C_1^- and C_2^- are small compared to the free eccentricity and have no noticeable effect on the evolution of R_b for Kepler-34 b.

The $1 + e_{AB}^2/2$ modification that we have just described is not rigorously correct. We have attempted to construct an analytic theory that is accurate to $O(e_{AB}^2)$. Preliminary analysis indicates that there are no additional corrections at $O(e_{AB}^2)$ for C_2^- but that there are additional corrections to the precession periods and C_1^- . The full $O(e_{AB}^2)$ corrections to the precession periods and C_1^- of Kepler-16 b and Kepler-35 b, as well as C_1^- of Kepler-34 b, remain small (less than a few %). For Kepler-35 b, the apsidal (nodal) precession period may decrease (increase) by a few years beyond the $1 + e_{AB}^2/2$ modification discussed above. The full $O(e_{AB}^2)$ theory also introduces new forced oscillation terms with frequencies $|kn_0 - (k \pm 2)n_{AB}|$, but they are likely small in amplitudes, as they are not observed in the direct numerical orbit integrations.

The most obvious effects of the gravitational force of the planet on the binary are the precession

of the binary’s periaipse and ascending node. Due to our choice of the invariable plane as the reference plane, the longitude of ascending node of the binary must be 180° from, and precesses at the same rate as, the longitude of ascending node of the planet. From the direct numerical orbit integrations, we find that the apsidal precession rates of the binary are 0.026, 0.0033 and 0.0086 degrees per year for Kepler-16, 34, and 35, respectively, which are much smaller than those of the planet. For the comparisons in §3, this very slow precession of the binary’s periaipse is taken into account by using ϖ_B from the numerical integrations when we plot R' defined in equation (44).

5. CONCLUSIONS

We have developed an analytic theory to model the motion of the recently discovered circumbinary planets: Kepler-16 b, Kepler-34 b, and Kepler-35 b. Their orbits are significantly non-Keplerian due to the large secondary-to-primary mass ratio and orbital eccentricity of the binaries, as well as the proximity of the planets to the binaries. The analytic theory in §2 shows that the motion in R and ϕ can be represented by the superposition of the circular motion of a guiding center at mean motion n_0 , the epicyclic motion, and the forced oscillations, and that the motion in z decouples from that in R and ϕ and has only free oscillations. One of the forced oscillation terms has frequency n_0 and can be identified as the forced eccentricity, while the epicyclic motion at frequency κ_0 can be identified as the free eccentricity.

Comparisons with direct numerical orbit integrations in §3 show that the analytic theory (with the simple modification in §4) gives an accurate description of the planetary motion for all three Kepler systems, including the precession of the periaipse and ascending node. The analytic theory explains the periodic variations in the amplitude of oscillations of the orbital radius (which is most obvious for Kepler-16 b and negligible for Kepler-34 b) by the superposition of the epicyclic motion and the forced eccentricity oscillation. The amplitude (and oscillating eccentricity) variations have a period equal to that of the apsidal precession as predicted by the theory.

The amplitude, C_1^- , of the forced eccentricity term is an explicit function of the parameters of the binary and of the guiding center radius of the planet in the analytic theory. For Kepler-16 b, 34 b, and 35 b, $C_1^- = 0.036$, 0.0019, and 0.0025, respectively. The free eccentricity, e_{free} , of the epicyclic motion is a free parameter in the analytic theory and can be obtained from, e.g., the variations in the orbital radius of the planet. For Kepler-16 b, 34 b, and 35 b, $e_{\text{free}} = 0.030$, 0.204, and 0.038, respectively. Note that the Kepler-34 system with the largest binary eccentricity ($e_{AB} = 0.52$) has the largest e_{free} while the other two Kepler systems with comparable e_{AB} have comparable e_{free} . Since the free eccentricity is a free parameter that was set by dynamical processes during the formation and/or subsequent evolution of the circumbinary planet, the free eccentricity of the three Kepler circumbinary planets (and additional circumbinary planets in the future) should provide important clues to these processes.

While this paper was under review, three more circumbinary planetary systems were an-

nounced: Kepler-38 and PH1 with one planet each and Kepler-47 with two planets (Orosz et al. 2012a,b; Schwamb et al. 2012). Direct numerical integrations and our analytic theory show that (i) Kepler-38 b is similar to Kepler-16 b in having $e_{\text{free}} \sim C_1^- \sim 0.024$ and large variations in the amplitude of oscillations in R ; (ii) Kepler-47 b is similar to Kepler-35 b in having e_{free} larger than $C_1^- \sim 0.004$ and moderate variations in the amplitude of oscillations in R ; (iii) Kepler-47 c is similar to Kepler-34 in having e_{free} much larger than $C_1^- \sim 0.001$ and negligible variations in the amplitude of oscillations in R ; and (iv) PH1 has $e_{\text{free}} \sim 0.1$ and $C_1^- \sim 0.04$.

It is a pleasure to thank Josh Carter for furnishing the best-fit orbital parameters of the Kepler circumbinary planetary systems, Daniel Fabrycky for informative discussions, and the referee for helpful comments on the manuscript. C. K. L. also thanks K. H. Chan, X. Tan, and W. Y. Li for enlightening discussion. This work was supported in part by Hong Kong RGC grant HKU 7034/09P.

REFERENCES

- Doyle, L. R., et al. 2012, *Science*, 333, 1602
- Goldreich, P., & Tremaine, S. 1980, *ApJ*, 241, 425
- Lee, M. H., & Peale, S. J. 2003, *ApJ*, 592, 1201
- Lee, M. H., & Peale, S. J. 2006, *Icarus*, 184, 573
- Murray, C. D., & Dermott, S. F. 1999, *Solar System Dynamics* (Cambridge: Cambridge Univ. Press)
- Orosz, J. A., et al. 2012a, *Science*, 337, 1511
- Orosz, J. A., et al. 2012b, *ApJ*, 758, 87
- Schwamb, M. E., et al. 2012, *ApJ*, submitted (arXiv:1210.3612)
- Welsh, W. F., et al. 2012, *Nature*, 481, 475
- Wisdom, J., & Holman, M. 1991, *AJ*, 102, 1528

Table 1. Orbital Parameters of Circumbinary Planetary Systems

Parameter	Kepler-16	Kepler-34	Kepler-35
Epoch (BJD)	2,455,000.0	2,454,900.0	2,454,900.0
GM_A (10^{-4} AU ³ d ⁻²)	2.0328	3.1045	2.6187
GM_B (10^{-4} AU ³ d ⁻²)	0.5987	3.0232	2.3903
GM_b (10^{-8} AU ³ d ⁻²)	9.3119	6.5822	3.6839
Binary star orbit			
Semimajor axis (AU)	0.22405	0.22847	0.17603
Eccentricity	0.16048	0.52068	0.14224
Inclination (deg)	0.0011	0.0020	0.0006
Argument of periapse (deg)	257.79	323.86	338.95
Long. ascending node (deg)	5.70	107.45	107.56
Mean anomaly (deg)	129.84	52.66	299.31
Planet orbit			
Semimajor axis (AU)	0.72042	1.08617	0.60497
Eccentricity	0.02373	0.20861	0.04845
Inclination (deg)	0.3083	1.8590	1.0714
Argument of periapse (deg)	304.05	69.41	91.17
Long. ascending node (deg)	185.70	287.45	287.56
Mean anomaly (deg)	358.85	17.75	292.17

Note. — The orbital parameters are the best-fit osculating Jacobian parameters relative to the invariable plane at the listed epoch.

Table 2. Parameters of Analytic Theory

Parameter	Kepler-16	Kepler-34	Kepler-35
R_0 (AU)	0.7016	1.0804	0.5933
n_K (yr $^{-1}$)	10.0823	8.0512	17.8875
n_0/n_K	1.00702	1.00423	1.00838
κ_0/n_K	0.99224	0.99567	0.99119
ν_0/n_K	1.02158	1.01272	1.02527
C_0	0.000159	0.000085	0.000131
C_1^0	−0.000282	$−6 \times 10^{-7}$	−0.000020
C_2^0	−0.000589	−0.000079	−0.000533
C_3^0	−0.000049	$−1 \times 10^{-7}$	−0.000003
C_1^+	0.000005	4×10^{-8}	3×10^{-7}
C_2^+	−0.000033	−0.000016	−0.000028
C_3^+	−0.000006	$−4 \times 10^{-8}$	$−4 \times 10^{-7}$
C_1^-	0.035772	0.001861	0.002493
C_2^-	0.002438	0.000683	0.001731
C_3^-	0.000110	7×10^{-7}	0.000007

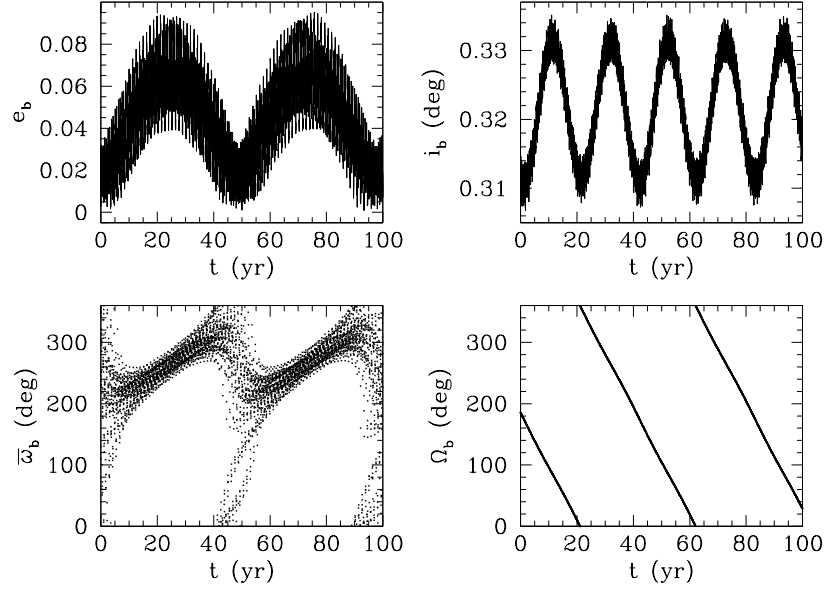


Fig. 1.— Evolution of the osculating Keplerian orbital elements (eccentricity e_b , inclination i_b , longitude of periape ϖ_b , and longitude of the ascending node Ω_b) of the planet Kepler-16 b over 100 yr from direct numerical orbit integration. The elements are relative to the center of mass of the binary, and the reference plane is the invariable plane.

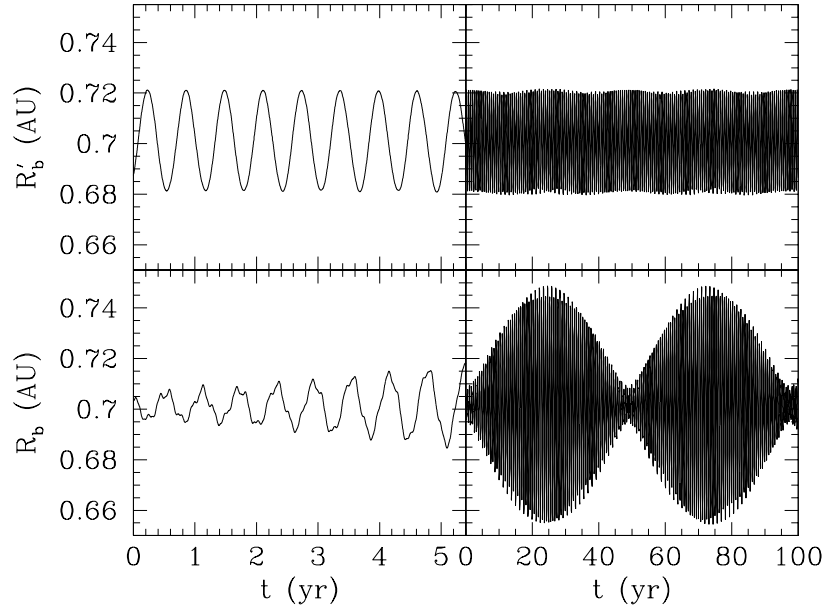


Fig. 2.— Variations in the orbital radius R_b (*bottom panels*) and the transformed orbital radius R'_b (*top panels*; eq. [44]) of the planet Kepler-16 b over several years (*left panels*) and over 100 yr (*right panels*) from direct numerical orbit integration.

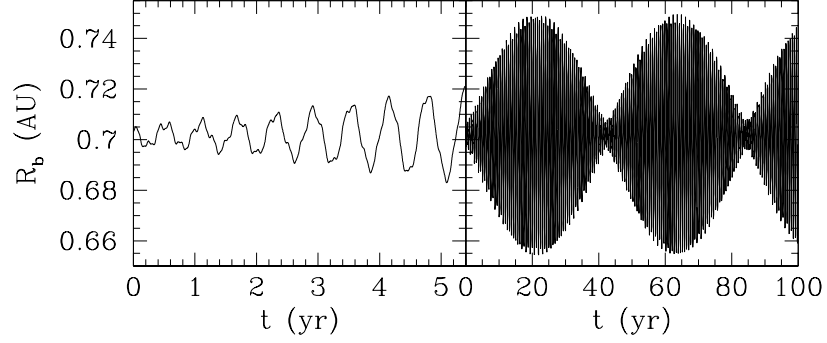


Fig. 3.— Variations in the orbital radius R_b of the planet Kepler-16 b over several years (*left panel*) and over 100 yr (*right panel*) according to equation (27) of the analytic theory with $e_{\text{free}} = 0.030$.

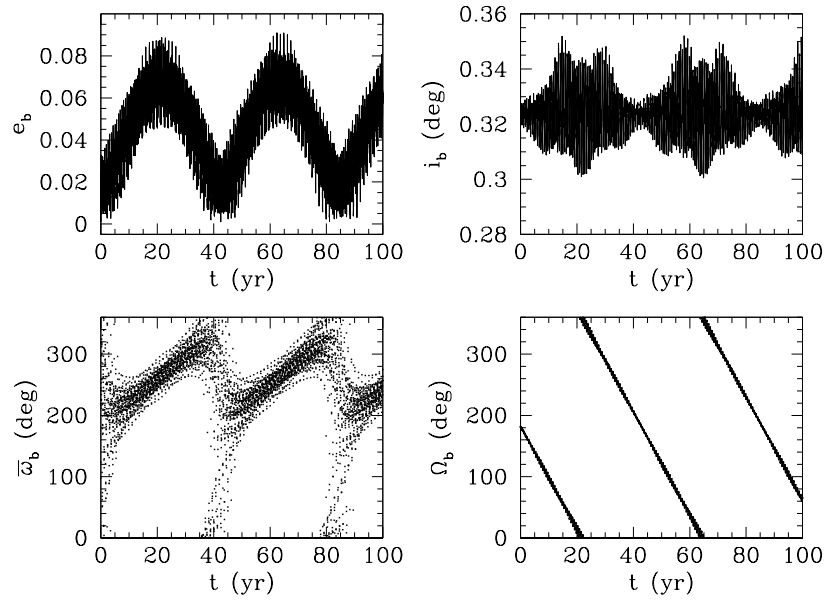


Fig. 4.— Same as Fig. 1, but according to the analytic theory with $e_{\text{free}} = 0.030$.

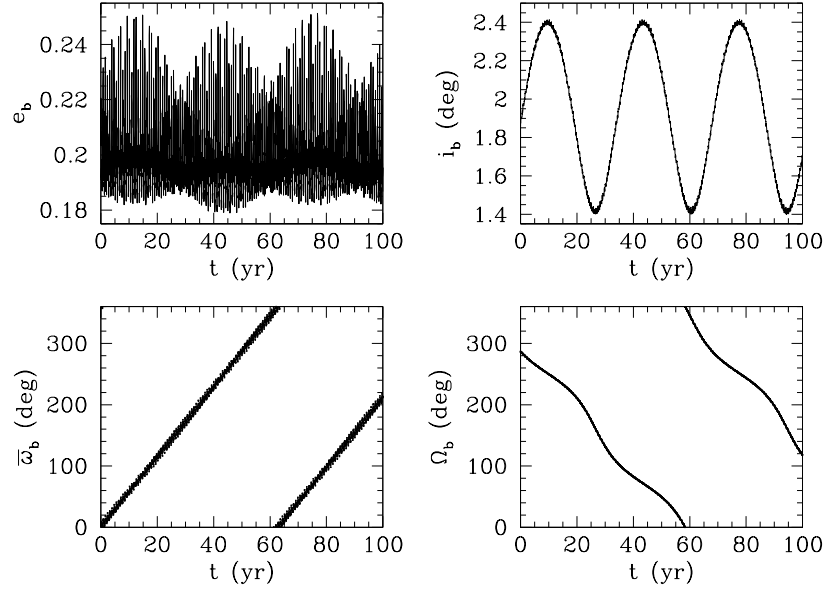


Fig. 5.— Same as Fig. 1, but for the planet Kepler-34 b.

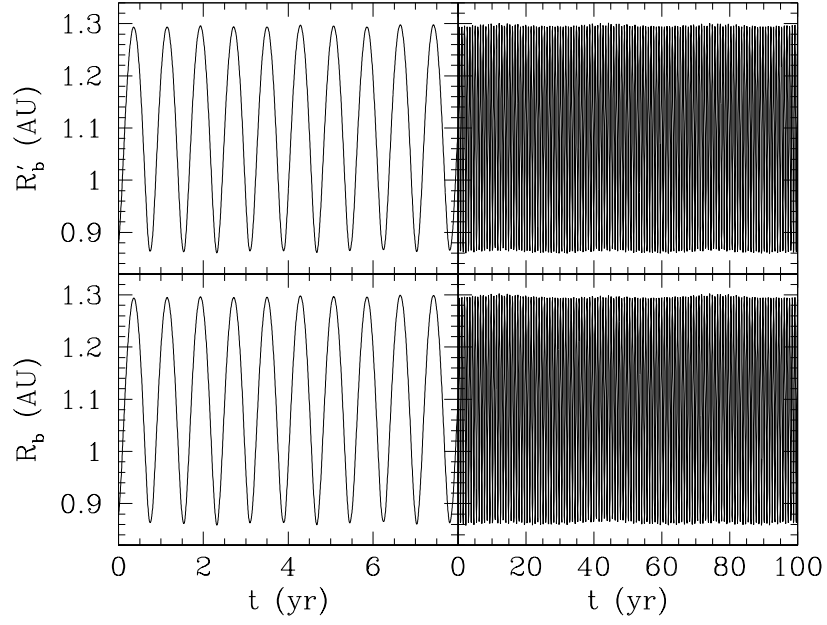


Fig. 6.— Same as Fig. 2, but for the planet Kepler-34 b.

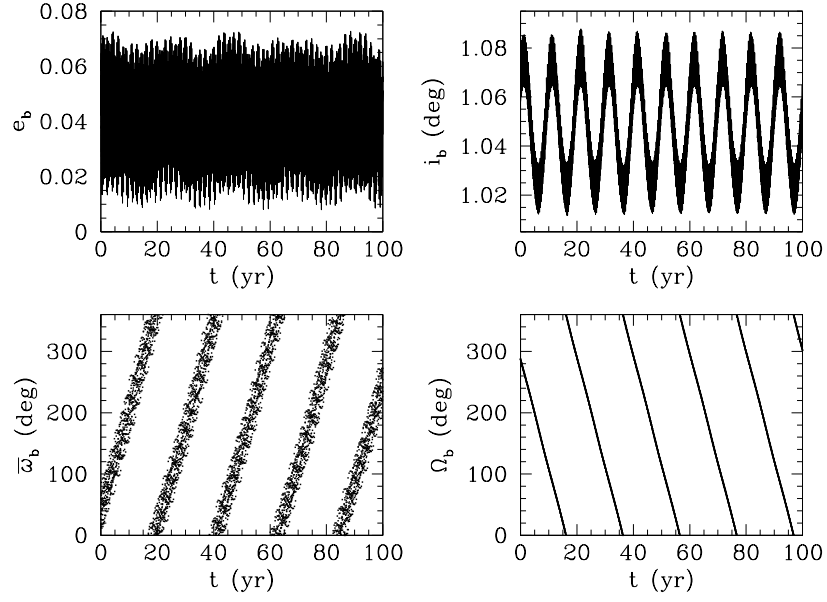


Fig. 7.— Same as Fig. 1, but for the planet Kepler-35 b.

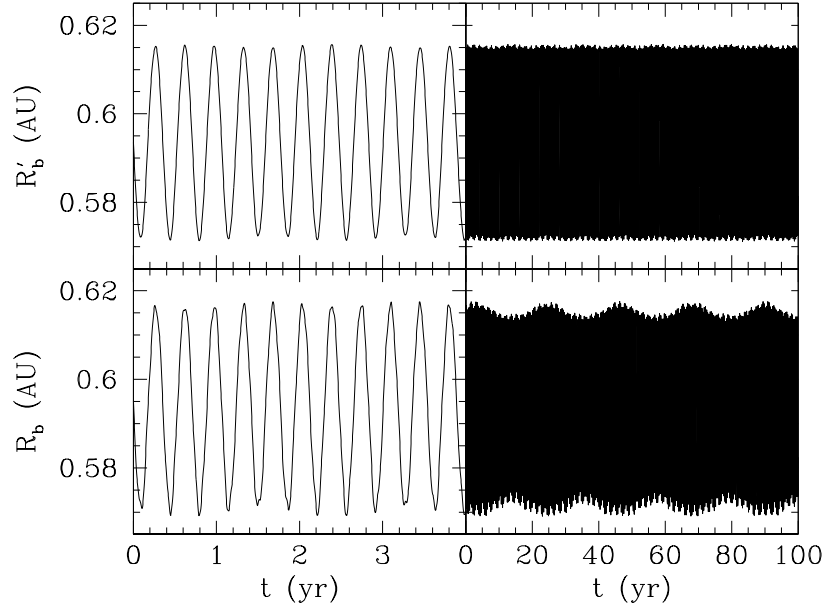


Fig. 8.— Same as Fig. 2, but for the planet Kepler-35 b.